SPANDIDOS PUBLICATIONS

ONCOLOGY REPORTS 49: 61, 2023

Use of time-density curves of dynamic contrast-enhanced computed tomography for determination of the histological therapeutic effects of neoadjuvant chemotherapy for pancreatic ductal adenocarcinoma

SHINTARO GOTO[1], TADASHI YOSHIZAWA[1], KEINOSUKE ISHIDO[2], HIROKO SEINO[3], SATOKO MOROHASHI[1], HIROKAZU OGASAWARA[2], SHUNSUKE KUBOTA[2], KENTA OGASAWARA[2], AKIE NAKAMURA[2], KENICHI HAKAMADA[2] and HIROSHI KIJIMA[1]

Departments of [1]Pathology and Bioscience and [2]Gastroenterological Surgery, Hirosaki University Graduate School of Medicine, Hirosaki, Aomori 036-8562; [3]Department of Radiology, Aomori National Hospital, Namioka, Aomori 038-1338, Japan

Received June 18, 2022; Accepted January 16, 2023

DOI: 10.3892/or.2023.8498

Abstract. The present study aimed to investigate the histological changes caused by neoadjuvant chemotherapy (NAC) for pancreatic ductal adenocarcinoma (PDAC), and to demonstrate the use of time-density curves (TDCs) of dynamic contrast-enhanced computed tomography (CECT) for determination of the histological therapeutic effects of NAC for PDAC. A total of 96 patients with PDAC were examined; 46 underwent NAC (NAC group) and 50 did not undergo NAC (non-NAC group). Based on histological therapeutic effect and using the area of residual tumor (ART) grading system, the NAC group was divided into low-responders and high-responders. Histological analysis was used to evaluate the densities of cancer cells, cancer-associated fibroblasts (CAFs), microvessels and stromal collagen fibers in the NAC and non-NAC groups. Radiological analysis was used to evaluate the TDCs of three slopes of the NAC group, namely slopes between the non-contrast and arterial phases (δ1 and δ1'), between the arterial and portal phases (δ2 and δ2'), and between the portal and equilibrium phases (δ3 and δ3'). δ1-δ3 were before NAC, whereas δ1'-δ3' were after NAC. Changes in δ1, δ2 and δ3 before and after NAC were denoted as δδ1 (=δ1'-δ1), δδ2 (=δ2'-δ2) and δδ3 (=δ3'-δ3). ART grading system, histological examination and radiological examination data were also statistically analyzed. Histological examination revealed a significant decrease in cancer cells and CAFs, and a significant increase in stromal collagen fibers due to NAC ($P<0.01$). Radiological examination revealed that δ1' was significantly higher than δ1 in low-responders ($P<0.05$), whereas δ2' was significantly lower than δ2 in high-responders ($P<0.01$). δδ2 was significantly lower and δδ3 was significantly higher in high-responders than in low-responders ($P<0.01$ and $P<0.05$, respectively). Receiver operating characteristic curve showed that δδ2 and δδ3 were effective indicators of the histological therapeutic effect of NAC. In conclusion, the TDC of dynamic CECT may be useful for determining the histological therapeutic effect of NAC for PDAC.

Correspondence to: Dr Tadashi Yoshizawa, Department of Pathology and Bioscience, Hirosaki University Graduate School of Medicine, 5 Zaifu-cho, Hirosaki, Aomori 036-8562, Japan
E-mail: tyoshi@hirosaki-u.ac.jp

Abbreviations: PDAC, pancreatic ductal adenocarcinoma; TDC, time-density curve; CECT, contrast-enhanced computed tomography; NAC, neoadjuvant chemotherapy; CAFs, cancer-associated fibroblasts; αSMA, α smooth muscle actin; ART, area of residual tumor

Key words: pancreatic cancer, PDAC, TDC, dynamic CECT, NAC, histological therapeutic effect, ART

Introduction

Pancreatic ductal adenocarcinoma (PDAC) is the most common histological type of pancreatic cancer, which is associated with chemoresistance (1). PDAC is characterized by desmoplastic stroma that includes α-smooth muscle actin (αSMA)-positive fibroblasts called cancer-associated fibroblasts (CAFs), which promote tumor growth and inhibit drug delivery (2,3). In recent years, neoadjuvant chemotherapy (NAC) has been accepted as a new standard strategy for the surgical management of PDAC (4,5). Furthermore, clinical trials have shown that surgery followed by chemotherapy provides better survival benefits than surgery alone (6). Similar to the conventional regimen of gemcitabine and S-1 (GS), a regimen of gemcitabine and nab-paclitaxel (GnP) has been reported to be associated with good outcomes in terms of progression-free survival and overall survival (7,8).

Although reports from clinical trials have been encouraging regarding the treatment of PDAC, there are limitations regarding the use of radiological examination and pathological

analysis for the determination of the therapeutic effects of NAC. Even though Response Evaluation Criteria in Solid Tumors is the accepted method for the determination of tumor progression, it may overestimate tumor burden (9). There are a number of grading systems used to determine the histological therapeutic effects of NAC, including the College of American Pathologists grading system, Evans grading system and MD Anderson Cancer Center grading system (10-12). However, it is difficult to compare grades between the systems because the grading systems use different criteria (13). Furthermore, radiological evaluation of treatment response using computed tomography (CT) or magnetic resonance imaging does not correspond to pathological results (14,15). Therefore, a new method of determination that integrates radiological and histological therapeutic effects is needed.

Our previous study on PDAC not treated with NAC showed that the time-density curve (TDC) of dynamic contrast-enhanced CT (CECT) was associated with the histological characteristics of PDAC, such as densities of cancer cells, CAFs and microvessels (16). Dynamic CECT consists of four time phases: Non-contrast, arterial, portal and equilibrium phases. TDCs represent serial changes in the contrast effect of tumors at the four time phases. Our previous study demonstrated that the first slope of the TDC between the non-contrast and arterial phases was associated with the density of microvessels, and that the second slope of the TDC between the arterial and portal phases was associated with the densities of cancer cells and CAFs. Based on our previous study, it was hypothesized that TDC changes before and after NAC may be associated with histological changes caused by NAC. The aim of the present study was to investigate the histological changes caused by NAC, and to demonstrate the use of TDC for the determination of the histological therapeutic effects of NAC for PDAC.

Materials and methods

Patients. A total of 96 patients with PDAC were examined; 46 underwent NAC (NAC group), whereas 50 did not undergo NAC (non-NAC group). The present study included a non-NAC group because a comparison between the NAC and non-NAC groups was necessary to understand the histological changes caused by NAC. Although it was possible to evaluate the histological therapeutic effects using specimens treated with NAC alone, evaluating the changes in cancer stroma and microvessels after NAC would be difficult if the treated specimens were not compared with non-treated specimens. The patients underwent surgical treatment at Hirosaki University Hospital (Hirosaki, Japan) between November 2011 and April 2021. Written informed consent for the use of clinical records and pathological specimens was obtained from each patient before commencement of the study. All of the patients underwent dynamic CECT; none of them had contrast media allergy or renal function problems that would prevent them from undergoing CECT. The NAC group underwent dynamic CECT before and after NAC. Pathological tumor, node and metastasis (TNM) categories and staging were conducted according to an up-to-date TNM classification from the Union for International Cancer Control (eighth edition) (17). Regarding histological differentiation, tumors were classified as well-differentiated, moderately differentiated or poorly differentiated according to the World Health Organization classification of tumors of the digestive system (fifth edition) (18). A total of 17 patients in the NAC group were administered 50 mg/m^2 S-1 on days 1-14 and 1,000 mg/m^2 gemcitabine on days 8 and 15 for two 21-day cycles (GS). A total of 29 patients in the NAC group were administered 75 mg/m^2 nab-paclitaxel, followed by 1,000 mg/m^2 gemcitabine on days 1, 8 and 15 for two 28-day cycles (GnP). For patients who received GS, the dosing period was 2-10 cycles. For patients who received GnP, the dosing period was 2-15 cycles (Tables SI and SII). The dosing periods were clinically determined based on preoperative stage and patient condition. At our institution, the usual dosing period for patients with resectable pancreatic cancer is two cycles of GS or GnP. In cases of locally advanced borderline pancreatic cancer, the dosing period was extended until surgical factors that may complicate radical resection, such as portal vein invasion or superior mesenteric nerve plexus invasion, were resolved. The clinicopathological characteristics of all patients, including age, sex, tumor location and dosing period of NAC, are summarized in Table I.

Method of determination of histological therapeutic effect. For the present study, the area of residual tumor (ART) grading system was adopted as the method of determination of histological therapeutic effect of NAC. The ART grading system was adopted because Matsuda *et al* (13) reported that this system was the most prognostic method for the determination of the histological therapeutic effects of NAC for PDAC, whereas other grading systems, such as the College of American Pathologists, Evans and MD Anderson Cancer Center grading systems, did not demonstrate significant associations with patient outcomes. In the present study, the largest cross-section of tumor tissue stained with hematoxylin and eosin (H&E) was evaluated in the NAC group according to the ART grading system using a BX53 light microscope (Olympus Corporation) with a 10x eyepiece and a 4x objective lens (UPlanSApo 4x; Olympus Corporation). High- and low-responders were defined as patients in whom the ART was less than or equal to three 40x microscopic fields, and greater than three 40x microscopic fields, respectively. Treatments for non-viable cancer cells and histological changes following NAC, including fibrosis, macrophage aggregates, vascular degeneration and acellular mucous pools, were adjusted in accordance with the criteria of the ART grading system. Notably, histological evaluation was performed by expert pathologists specializing in pancreatobiliary pathology (TY and HK). Furthermore, all histological evaluations were performed while these pathologists were blinded to the clinical information.

Surgical specimens. The surgical specimens of the NAC and non-NAC groups were examined. In our hospital, we routinely sample whole PDAC tissues for pathological diagnosis. In the NAC group, 27 patients underwent pancreatoduodenectomy and 19 patients underwent pancreatosplenectomy. In the non-NAC group, 26 patients underwent pancreatoduodenectomy and 24 patients underwent pancreatosplenectomy. No patient underwent total pancreatectomy. Surgical specimens from pancreatoduodenectomy were sliced axially, whereas

Table I. Clinicopathological characteristics of NAC-treated group and NAC-untreated group.

Parameter	NAC-treated group	Non-NAC group	P-value
Number of patients	46	50	
Age, years			0.237
≤65	20	22	
>65	26	48	
Sex			0.683
Male	23	22	
Female	23	28	
Location, n (%)			0.543
Head	27 (58.7)	26 (52.0)	
Body or tail	19 (41.3)	24 (48.0)	
Histological differentiation, n (%)			0.772
Well	3 (6.5)	5 (10.0)	
Moderate	39 (84.8)	42 (84.0)	
Poor	4 (8.7)	3 (6.0)	
Pathological T stage, n (%)			0.758
T1	17 (37.0)	16 (32.0)	
T2	27 (58.7)	30 (60.0)	
T3	2 (4.3)	4 (8.0)	
Pathological N stage, n (%)			0.575
N0	24 (52.2)	32 (64.0)	
N1	19 (41.3)	16 (32.0)	
N2	3 (6.5)	2 (4.0)	
Clinical M stage, n (%)			1.000
M0	46 (100)	50 (100)	
M1	0 (0)	0 (0)	
TNM stage, n (%)			0.341
Stage I	16 (34.8)	23 (46.0)	
Stage II	21 (45.7)	22 (44.0)	
Stage III	9 (19.5)	5 (10.0)	
Stage IV	0 (0)	0 (0)	
NAC, n (%)			1.000
GS	17 (37.1)	0 (0)	
GnP	29 (62.9)	0 (0)	
Dosing period cycles			
GS	2-10	0	
GnP	2-15	0	

GnP, gemcitabine and nab-paclitaxel; GS, gemcitabine and S-1; NAC, neoadjuvant chemotherapy; TNM, tumor, node, and metastasis.

surgical specimens from pancreatosplenectomy were sliced at right angles to the main pancreatic duct. All surgical specimens were fixed with 10% formalin at 24˚C for 24 h. Tissues were embedded in paraffin and sliced to a thickness of 4 μm for H&E staining and immunohistochemistry. H&E staining was performed using Mayer's hematoxylin for 20 min and with eosin for 5 min.

Histological image analysis. The histological characteristics of the NAC and non-NAC groups were investigated. The densities of cancer cells, CAFs, microvessels and stromal collagen fibers in the whole areas of the tumor were measured in a way similar to that described in our previous study (16). In the non-NAC group, the entire maximum cross-section of the tumor was examined. In the NAC group, ARTs, including viable cancer cells, were examined. Maximum cross-sections of tumor were divided into 40x microscopic fields using a BX53 light microscope with a 10x eyepiece and a 4x objective lens (UPlanSApo 4x) and a DP74 digital camera (Olympus Corporation). Whole images of the largest cross-sections of tumors with immunohistochemistry and Masson's trichrome staining were captured using CellSens software (version 2.3 64-bit; Olympus Corporation).

In the present study, ImageJ software [Java 1.6.0_24 (64-bit); National Institutes of Health] was used to analyze the histological images following immunohistochemistry and Masson's trichrome staining. The area of cytokeratin AE1/AE3, αSMA and CD31-positive components was measured in terms of the pixel number using thresholds with minimum and maximum values of 0 and 120, respectively. Finally, the average area ratios of positive components in the whole largest cross-sections of tumors were measured as the densities of cancer cells, CAFs, microvessels and stromal collagen fibers.

Immunostaining and Masson's trichrome staining. To measure the densities of cancer cells, CAFs, microvessels and stromal collagen fibers, immunohistochemistry (cytokeratin AE1/AE3, αSMA and CD31) and Masson's trichrome staining were performed on the slides of the maximum cross-section of the tumor. Cytokeratin AE1/AE3 is positive in cancer cells and nontumoral epithelial cells. αSMA is used as a general marker of CAFs in numerous types of human cancer (19-21). CD31 is positive in vascular endothelial cells of tumoral and nontumoral vessels (22). In the present study, Masson's trichrome staining was used to measure the density of stromal collagen fibers because it provides better visualization than immunohistochemistry (23).

Tissue slides were deparaffinized using the avidin-biotin-peroxidase complex method with Benchmark XT autoimmunostainer (Roche Tissue Diagnostics; Roche Diagnostics, Ltd.). Deparaffinized slides were treated with tris-EDTA buffer (pH 7.8) at 95˚C for 44 min. The slides were then treated with 5% non-fat dry milk at 37˚C for 15 min to block endogenous peroxides and proteins. Subsequently, the slides were incubated with primary antibodies for 60 min at 24˚C. The clone numbers and dilution ratios of the primary antibodies were as follows: Cytokeratin AE1/AE3 (monoclonal mouse; clone AE1, AE3; 1:100; cat. no. 412811; Nichirei Bioscience Inc.), αSMA (monoclonal mouse; clone 1A4; cat. no. M0851; 1:100; Dako; Agilent Technologies, Inc.) and CD31 (monoclonal mouse; clone JC70A; cat. no. M0823; 1:40; Dako; Agilent Technologies, Inc.). All reaction products of primary antibodies were visualized using the iVIEW DAB detection kit with a biotin-conjugated goat anti-mouse immunoglobulin G secondary antibody (1:1,000; cat. no. 760-091; Roche Tissue Diagnostics; Roche Diagnostics, Ltd.). Slides were incubated with the secondary antibody at 37˚C for 1 h. Subsequently, counterstaining with hematoxylin at 37˚C for 8 min was performed and staining was observed under an optical microscope.

For Masson's trichrome staining, tissue slides were deparaffinized and rehydrated in 100, 95 and 70% alcohol. After washing in distilled water, the slides were stained in Weigert's iron hematoxylin working solution for 10 min. After further washing in distilled water, slides were stained in 1% Biebrich scarlet-acid fuchsin solution for 15 min. Slides were then differentiated in 5% phosphomolybdic-phosphotungstic acid solution after washing in distilled water. Subsequently, slides were directly stained in aniline blue solution for 10 min without rinsing. After washing in distilled water, slides were differentiated in 1% acetic acid solution for 5 min. After further washing in distilled water, slides were dehydrated quickly in 95% ethanol and cleared in xylene. Masson's trichrome staining was performed at 24˚C and staining was observed under an optical microscope.

Radiological imaging analysis. All of the patients in the NAC group underwent dynamic CECT before and after NAC using the fixed protocol at Hirosaki University Hospital. The protocol was the same as that described in our previous study (16). Dynamic CECT was conducted using a 64-detector row CT scanner (Discovery CT750 HD; GE Healthcare) with the following parameters: Detector configuration of 64x0.625, tube voltage of 120 kV, automatic tube current modulation, collimation of 40 mm, tube rotation time of 0.5 sec, pitch of 0.8, field of view of 35x35 cm, image matrix of 512x512, and slice thickness of 5 mm. After obtaining unenhanced images, a non-ionic contrast medium dose of 600 mgI/kg body weight with an iodine content of 300 mgI/ml (Iopamiron 300/370, Bayer Yakuhin Ltd.; Omnipaque 300, Daiichi-Sankyo Co. Ltd.; Iopromide 300/370, Fujifilm Toyama Chemical Co., Ltd.; Iomelon 350, Eisai Co. Ltd.; Optiray 320, Fuji Pharma Co., Ltd.) was injected intravenously within 30 sec, and scanning of the arterial, portal venous and equilibrium phases began 35-40, 60-70 and 180 sec after the start of contrast medium injection.

TDCs were drawn using Digital Imaging and Communications in Medicine data [EV insite R version 3.4.0.0 (PSP Corporation); or ShadeQuest/ViewR V1.24 (Yokogawa Medical Solutions)]. The method used to draw regions of interest (ROIs) in our previous study was used in the present study (16). The ROIs were drawn on the central areas of tumors, avoiding tumor margins, contrasted vessels and artificial materials, such as stents. Tumor margins were avoided in ROIs because histological analysis excluded tumor margins since they included a number of nontumoral components. After measuring the number of ROIs on CT for each time phase, the digital imaging software created TDCs before and after NAC. At our institution, all patients with PDAC underwent dynamic CECT via a fixed protocol to limit the influence of patient-related factors, such as body weight, and cardiac and renal function, which can affect TDCs. Additionally, concentrations of contrast agents and their administration rates were adjusted according to patient body weight, and cardiac and renal function. However, all patient-related factors could not be completely controlled. Therefore, in the present study, the slopes of the TDC were adopted as parameters of radiological images to minimize error factors because we considered that the changes in the rates of contrast enhancement were more appropriate than individual CT values. δ1 was defined as the first slope between the non-contrast and arterial phases before NAC, δ2 was defined as the second slope between the arterial and portal phases before NAC, and δ3 was defined as the third slope between the portal and equilibrium phases before NAC. δ1' was defined as the first slope after NAC, δ2' was defined as the second slope after NAC, and δ3' was defined as the third slope after NAC. δδ1 was defined as δ1' minus δ1, δδ2 was defined as δ2' minus δ2, and δδ3 was defined as δ3' minus δ3. CT number [in Hounsfield unit (HU)] was plotted on the vertical axis of the TDC, and time phase was plotted on the horizontal axis of the TDC.

Table II. Clinicopathological characteristics of NAC group.

Parameter	Low-responder	High-responder	P-value
Number of patients	29	17	
Age, years			0.533
≤65	10	8	
>65	19	9	
Sex			0.542
Male	16	7	
Female	13	10	
Location, n (%)			0.028
Head	21 (72.4)	6 (35.3)	
Body or tail	8 (27.6)	11 (64.7)	
Histological differentiation, n (%)			0.193
Well	1 (3.4)	2 (11.8)	
Moderate	24 (82.8)	15 (88.2)	
Poor	4 (13.8)	0 (0)	
Pathological T stage, n (%)			0.498
T1	9 (31.0)	8 (47.1)	
T2	18 (62.1)	9 (52.9)	
T3	2 (6.9)	0 (0)	
Pathological N stage, n (%)			0.504
N0	16 (55.2)	8 (47.1)	
N1	10 (34.5)	9 (52.9)	
N2	3 (10.3)	0 (0)	
Clinical M stage, n (%)			1.000
M0	29 (100)	17 (100)	
M1	0 (0)	0 (0)	
TNM stage, n (%)			
Stage I	9 (31.0)	7 (41.2)	0.245
Stage II	12 (41.4)	9 (52.9)	
Stage III	8 (27.6)	1 (5.9)	
Stage IV	0 (0)	0 (0)	
NAC, n (%)			1.000
GS	11 (37.9)	6 (35.3)	
GnP	18 (62.1)	11 (64.7)	
Dosing period, cycles			
GS	2-8	2-10	
GnP	2-12	2-15	

GnP, gemcitabine and nab-paclitaxel; GS, gemcitabine and S-1; NAC, neoadjuvant chemotherapy; TNM, tumor, node, and metastasis.

Statistical analysis. First, comparisons of the densities of cancer cells, CAFs, microvessels and stromal collagen fibers between the non-NAC group, low-responders and high-responders were examined using the Kruskal-Wallis test, followed by the Steel-Dwass post hoc test. Second, the differences between δ1 and δ1', δ2 and δ2', and δ3 and δ3' in low-responders and high-responders were analyzed using Wilcoxon test. Third, differences in δδ1, δδ2 and δδ3 between low-responders and high-responders were analyzed using Mann-Whitney U-test, which was also used for comparison of CAFs and microvessels, A receiver operating characteristic curve was drawn to calculate the cutoff value of radiological parameters between low- and high-responders. Furthermore, Kaplan-Meier curves and log-rank test were used to analyze recurrence-free survival according to the ART grading system and radiological parameters. Contingency tables were analyzed using Fisher's exact test.

All statistical analyses were performed using EZR version 1.54 (Saitama Medical Center, Jichi Medical University, Saitama, Japan), which is a modified version of R commander designed to add statistical functions frequently used in biostatistics (24).

Results

Clinicopathological characteristics of the NAC group. The ART grading system classified 29 patients as low-responders and 17 patients as high-responders. The clinicopathological characteristics of the NAC group are summarized in Table II using Pearson's chi-square test.

Results of histological analysis. The ART grading system classified the NAC group into high-responders and low-responders. High-responders had ARTs less than or equal to three 40x microscopic fields. Low-responders had ARTs greater than three 40x microscopic fields (Fig. 1).

At the time of analyzing histological images, cytokeratin AE1/AE3 was positive in cancer and nontumoral epithelial cells on tumor margins. Nontumoral epithelial cells were excluded following H&E staining. Even though αSMA was positive in CAFs and vascular smooth muscles, Mann-Whitney U-test showed that the number of CAFs was significantly greater than the number of vascular smooth muscles in the NAC and non-NAC groups (data not shown). Therefore, the effect of smooth muscles on the measurement were ignored because the number of CAFs was predominantly greater than the number of vascular smooth muscles.

Immunohistochemical analysis revealed a marked decrease in cancer cells (Fig. 2B and G) and CAFs (Fig. 2C and H) in the high-responders compared with those in the low-responders and non-NAC group (Fig. 2). Kruskal-Wallis test revealed that the density of cancer cells was significantly decreased in order from the non-NAC group to low-responders to high-responders (Fig. 3A). Similarly, the density of CAFs was significantly decreased in order from the non-NAC group to low-responders to high-responders (Fig. 3B). There were no significant differences in the density of microvessels between the non-NAC group, low-responders and high-responders (Fig. 3C). Furthermore, collagen fiber density was significantly increased in the NAC groups compared with that in the non-NAC group; however, there was no significant difference in collagen fiber density between low-responders and high-responders (Fig. 3D).

Results of radiological analysis. The curve shape of the TDC was markedly altered before and after NAC (Fig. 4). In low-responders, δ1' was significantly higher than δ1 (Fig. 5A), whereas there were no significant differences between δ2 and δ2' (Fig. 5B). δ3' was significantly lower than δ3 (Fig. 5C). In high-responders, there was no significant difference between δ1 and δ1' (Fig. 5D), δ2' was significantly lower than δ2 (Fig. 5E), and there was no significant difference between δ3 and δ3' (Fig. 5F). No significant difference was noted in δδ1 between low-responders and high-responders (Fig. 5G). Furthermore, δδ2 was significantly lower and δδ3 was significantly higher in high-responders than in low-responders (Fig. 5H and I). Receiver operating characteristic curve showed that the cutoff values between low-responders and high-responders were δδ2=-3.448 HU/sec [sensitivity=82.4%, specificity=69.0%, area under the curve (AUC)=0.775] and δδ3=4.983 HU/sec (sensitivity=58.8%, specificity=89.7%, AUC=0.718) (Fig. 6). Regarding the ART grading system, there was no prognostic significant difference between high- and low-responders (P=0.166). In addition, there was no prognostic significant difference between high and low δδ2; the cutoff value of δδ2 was -3.448 HU/sec. Furthermore, there was no prognostic significant difference between high and low δδ3; the cutoff value of δδ3 was 4.983 HU/sec (Fig. 7).

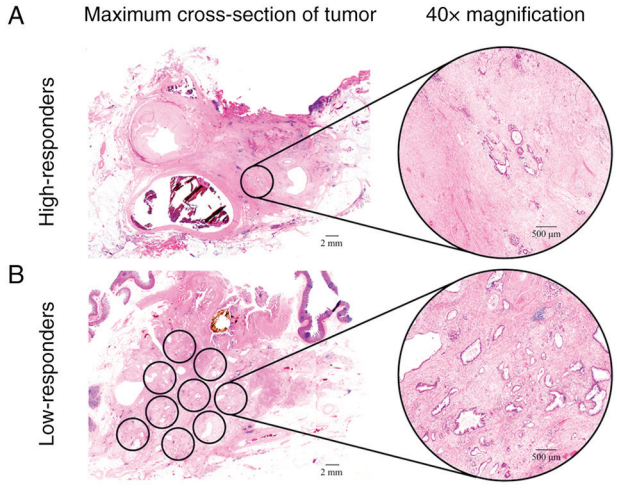

Figure 1. Representative cases of high-responders and low-responders based on the ART grading system. (A) High-responders have ARTs less than or equal to three 40x microscopic fields. The image on the left is a representative low-magnification (12.5x) image of the high-responders; the image on the right is magnified (40x). This case presented with only one 40x microscopic field of residual tumor (round circled area). (B) Low-responders have ARTs greater than three 40x microscopic fields. The image on the left is a representative low-magnification (12.5x) image of the low-responders; the image on the right is magnified (40x). This case presented with nine 40x microscopic fields of residual tumor (round circled areas). ART, area of residual tumor.

Discussion

In the present study, the histological differences between the NAC and non-NAC groups, and the association between the TDC and histological therapeutic effects were investigated. Histological examination revealed that NAC effectively reduced the densities of cancer cells and CAFs, and significantly increased the density of stromal collagen fibers. Radiological and histological examinations suggested that δδ2 and δδ3 were associated with a high histological therapeutic effect based on the ART grading system. Furthermore, the present study suggested the potential use of TDCs for the prediction of the histological therapeutic effect of NAC for PDACs.

Comparison of the histological characteristics of the NAC and non-NAC groups revealed that NAC reduced the densities of cancer cells and CAFs, and increased the density of stromal collagen fibers. In the present study, >50% of the NAC group consisted of patients who underwent NAC with GnP. Miyashita *et al* reported that NAC with GnP reduced the density of CAFs in patients with PDAC, thereby depleting the tumor stroma (25). Although this study did not focus on NAC with GnP, it is possible that the strong resistance of tumor stroma against GnP is associated with the reduction in the density of CAFs, given that patients who underwent NAC with GnP made up 63% of the NAC group. Furthermore, an overwhelming proliferation of stromal collagen fibers was

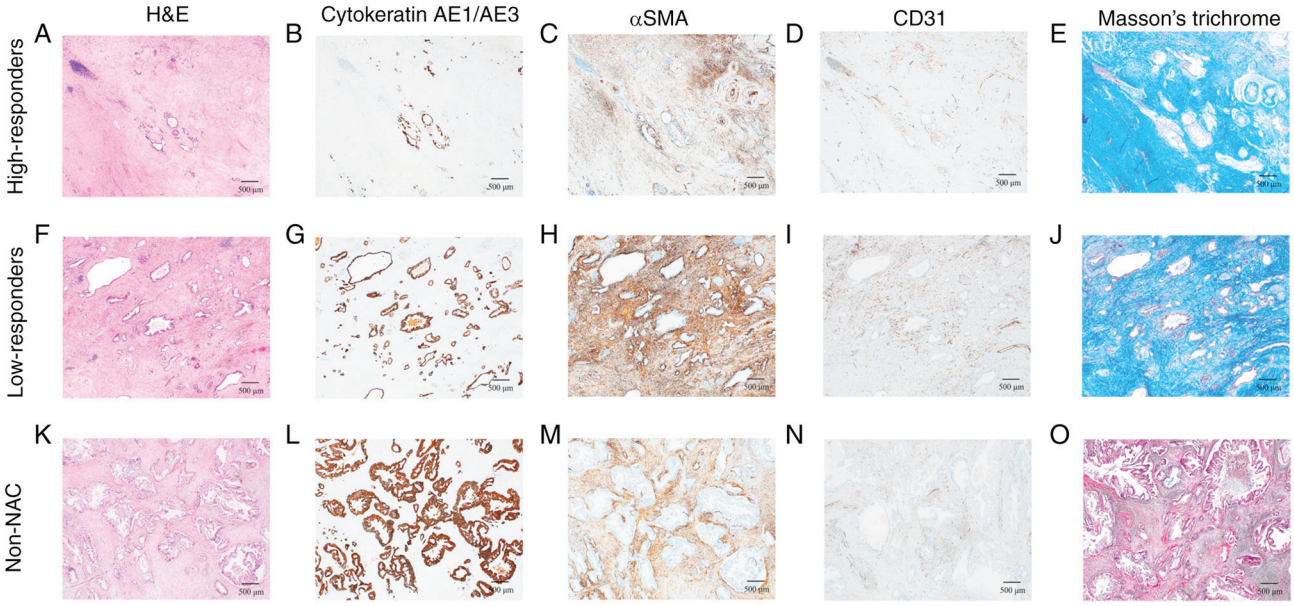

Figure 2. Representative histological characteristics of the high-responders, low-responders and non-NAC group. Cytokeratin AE1/AE3 was positive in cancer cells, αSMA was positive in CAFs, and CD31 was positive in microvessels. Masson's trichrome stain was used for staining the collagen fibers. High-responders exhibited a marked decrease in cancer cells and CAFs. Low-responders showed a slight decrease in cancer cells. High-responders' microscopic images (40x magnification) of (A) H&E staining, (B) cytokeratin AE1/AE3, (C) αSMA, (D) CD31 immunostaining, and (E) Masson's trichrome stain. Low-responders' microscopic images (40x magnification) of (F) H&E staining, (G) cytokeratin AE1/AE3, (H) αSMA, (I) CD31 immunostaining, and (J) Masson's trichrome stain. Non-NAC group's microscopic images (40x magnification) of (K) H&E staining, (L) cytokeratin AE1/AE3, (M) αSMA, (N) CD31 immunostaining, and (O) Masson's trichrome stain. αSMA, α-smooth muscle actin; CAF, cancer-associated fibroblast; H&E, hematoxylin and eosin; NAC, neoadjuvant chemotherapy.

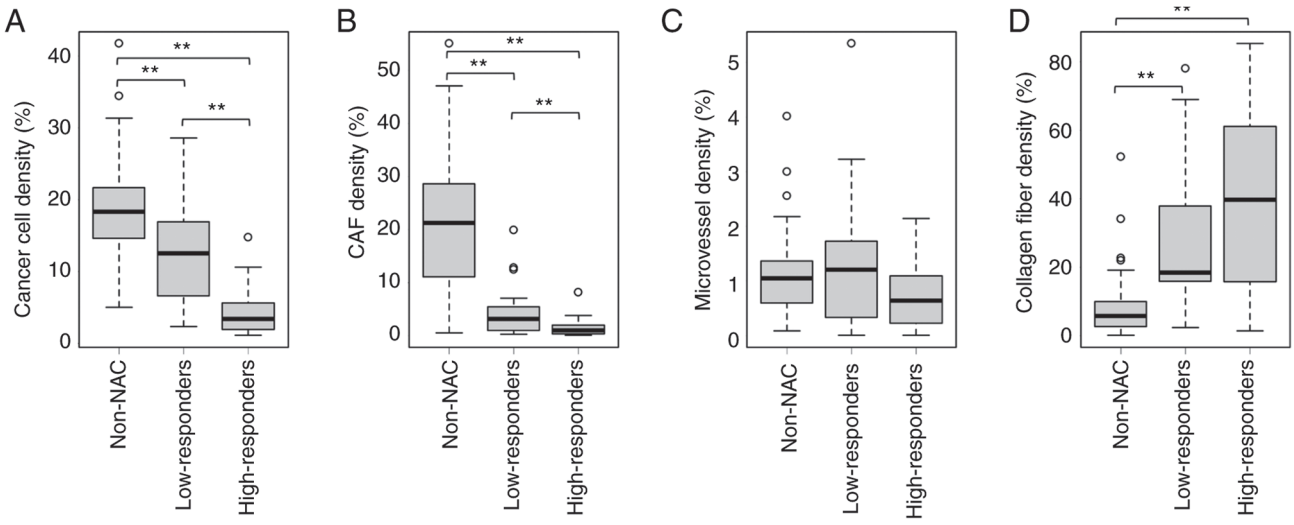

Figure 3. Results of histological examination between the non-NAC group, low-responders and high-responders. (A) Cancer cell density was significantly decreased in order from the non-NAC group to low-responders to high-responders. (B) CAF density was significantly decreased in order from the non-NAC group to low-responders to high-responders. (C) There was no significant difference in microvessel density between the non-NAC group, low-responders and high-responders. (D) Collagen fiber density was significantly higher in the NAC group than in the non-NAC group. There was no significant difference in collagen fiber density between low-responders and high-responders. **P<0.01. CAFs, cancer-associated fibroblasts; NAC, neoadjuvant chemotherapy.

observed in the NAC group. Tissues exposed to chemotherapy undergo a wound-healing process that involves deposition of extracellular matrix, which includes various types of collagen fibers (26). An association between microvessel density and NAC was not revealed in the present study. It was reported in several previous studies that treatment with NAC and anti-vascular endothelial growth factor drugs, such as bevacizumab, can reduce microvessel density in primary and metastasized rectal cancer (27,28). However, to the best of our knowledge, there are no studies on PDAC that investigated the association between NAC and microvessel density.

Comparison of TDCs before and after NAC revealed that δ1' was significantly higher than δ1 in low-responders. In our previous study, it was revealed that the first slope of TDCs is associated with microvessel density (16). Even though there were no significant differences in microvessel density between

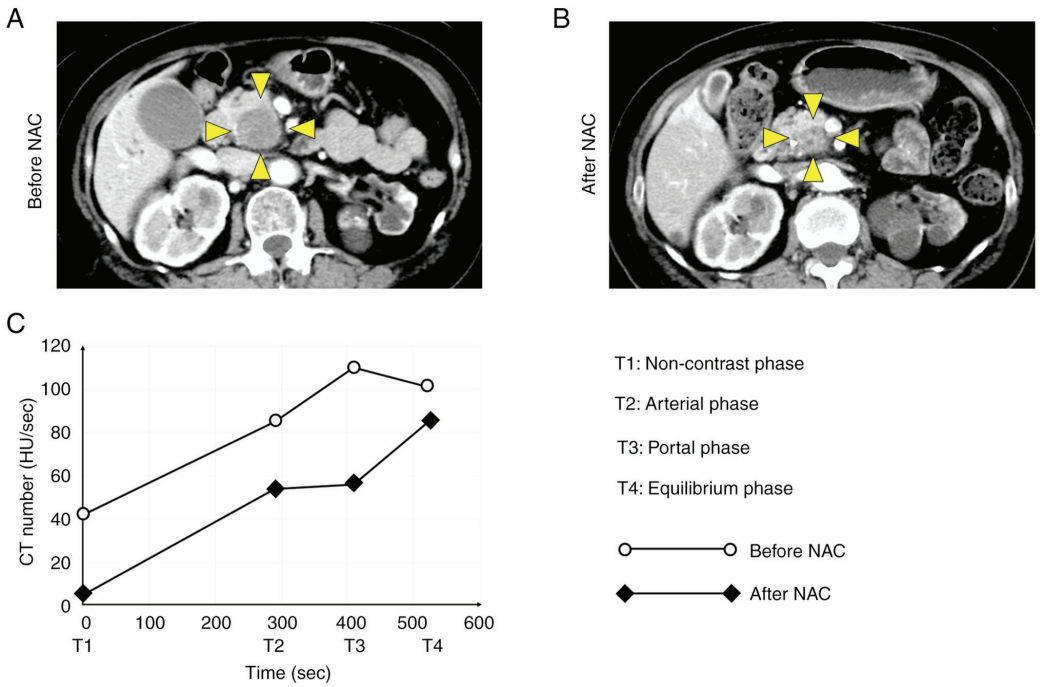

Figure 4. Representative radiological analysis of high-responders' TDC before and after NAC. The curve shape was markedly altered before and after NAC. (A and B) Dynamic CECT image of PDAC before and after NAC. The tumor demonstrates low-density areas (surrounded by yellow arrow heads). (C) TDC drawn from dynamic CECT before and after NAC. Both TDCs before and after NAC comprise four time phases: Non-contrast (T1), arterial (T2), portal (T3) and equilibrium phases (T4). CECT, contrast-enhanced computed tomography; HU, Hounsfield unit; NAC, neoadjuvant chemotherapy; TDC, time-density curve.

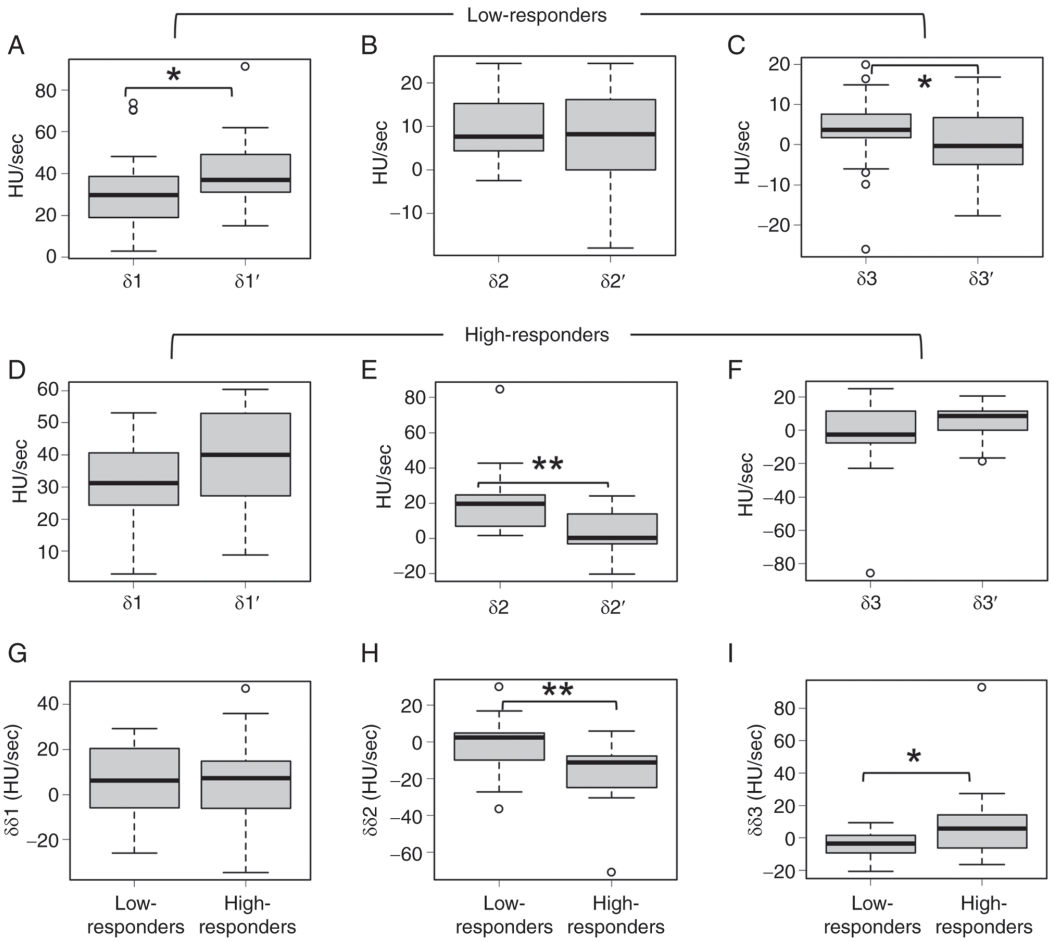

Figure 5. Association between time-density curves and the area of residual tumor grading system. (A) δ1 and δ1', (B) δ2 and δ2', and (C) δ3 and δ3' in low-responders. (D) δ1 and δ1', (E) δ2 and δ2', and (F) δ3 and δ3' in high-responders. Differences in (G) δδ1, (H) δδ2 and (I) δδ3 between low- and high-responders. $^{*}P<0.05$, $^{**}P<0.01$.

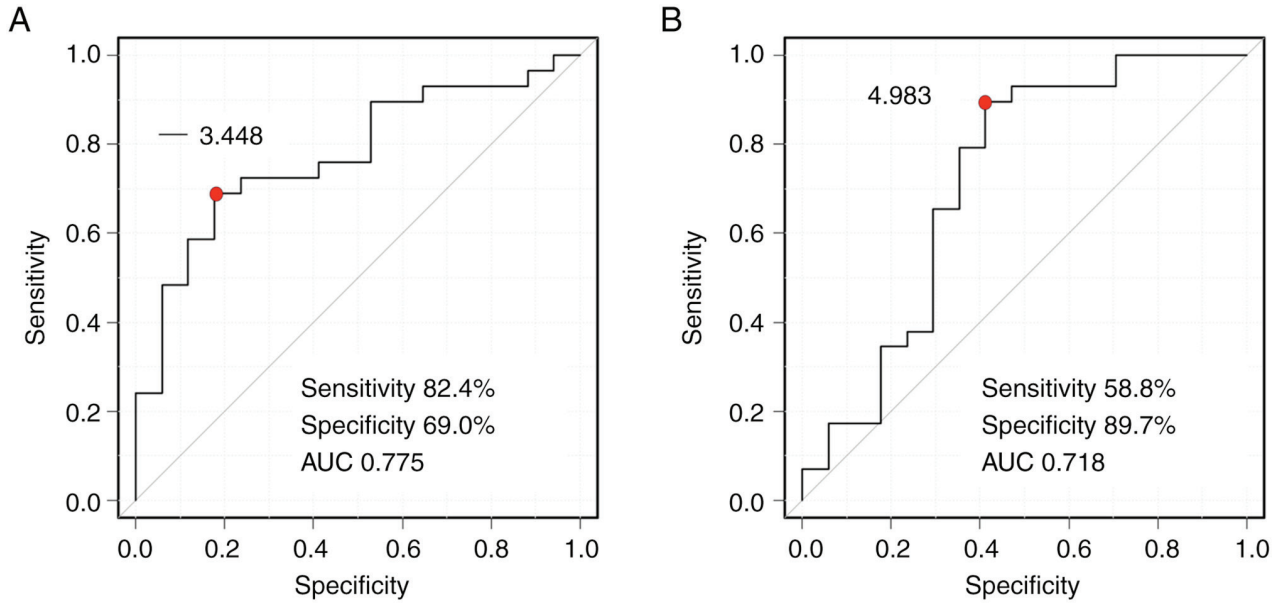

Figure 6. ROC curves of δδ2 and δδ3. (A) ROC curve of δδ2. The cutoff value of δδ2 between low-responders and high-responders was-3.448 HU/sec (sensitivity=82.4%, specificity=69.0%, AUC=0.775). (B) ROC curve of δδ3. The cutoff value of δδ3 between low-responders and high-responders was 4.983 HU/sec (sensitivity=58.8%, specificity=89.7%, AUC=0.718). AUC, area under the curve; HU, Hounsfield unit; ROC, receiver operating characteristic.

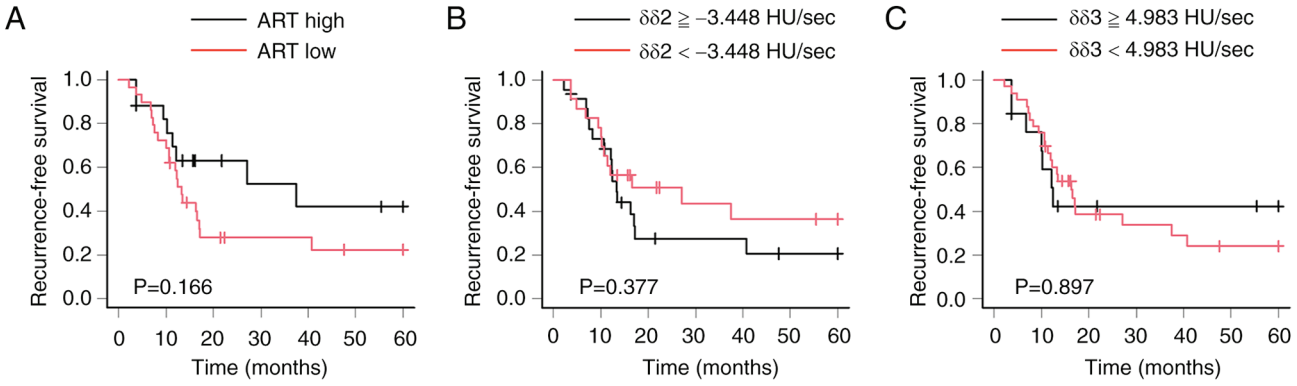

Figure 7. Kaplan-Meier curves for recurrence-free survival according to the (A) ART grading system, (B) δδ2 and (C) δδ3. ART, area of residual tumor; HU, Hounsfield unit.

low-responders and high-responders, tumor angiogenesis may have involved the ascent of the first slope of TDC in low-responders. In high-responders, δ2' was significantly lower than δ2. Moreover, δδ2 was significantly lower and δδ3 was significantly higher in high-responders compared with that in low-responders. In our previous study, it was reported that the second slope of TDC (δ2) is associated with tumor cellularity, including the densities of cancer cells and CAFs (16). The lower δδ2 and the higher δδ3 in high-responders compared with low-responders may be because abundant collagen fibers replace cancer cells and CAFs in stromal areas. Non-ionic contrast agents are typically used for the diagnosis of pancreatic cancer. They do not distribute into the cytoplasm of cancer cells and CAFs, but they do distribute into the extracellular matrix (29). In general, they leak from microvessels into the intracellular matrix of tumors between the arterial and portal phases. Stromal collagen fiber proliferation may have strongly suppressed the leak of contrast agents from microvessels into intracellular matrix, thereby lowering the δδ2. Contrast agents are generally resorbed into microvessels across a concentration gradient between the portal and equilibrium phases. Furthermore, stromal collagen fiber proliferation may have strongly suppressed the resorption of contrast agents from intracellular matrix into microvessels, leading to an increased δδ3. It was hypothesized that the decrease in the second slope and the increase in the third slope in high-responders are not independent phenomena but are sequential phenomena associated with NAC-induced stromal collagen fiber proliferation.

The predictive value of tumor markers (such as CA19-9), PET-CT, perfusion CT and CECT have been reported when predicting treatment response to NAC for PDAC in previous studies (30-33). Although the predictive values were interesting, the sample sizes of the previous studies were smaller than that of the present study. Additionally, some studies lacked a detailed description of the histological effects following therapy. A previous study used the Evans grading system

to evaluate the histological response to NAC. Although this system is considered a standard method, it is ambiguous (11). Furthermore, as it specifies a percentage of tumor cell viability or destruction, it is difficult to determine the viability of degenerative tumor cells (13). In the present study, the ART grading system and simpler criteria were adopted, which enabled the detection of cases with an excellent response to NAC. In addition to the advantages of using the ART grading system, the present study investigated the histological characteristics of PDAC with/without NAC using immunohistochemistry. It was revealed that NAC-induced intense changes in PDAC stroma, because the NAC groups showed a decrease in CAFs and increase in collagen fibers in the cancer stroma compared with in the non-NAC group. However, it is difficult to confirm the stromal changes that affected the TDC. The results of the present study suggest an association between the changes in TDC and histological changes after NAC by performing radiological and histological analyses.

The present study has some limitations. First, although it was suggested that the proliferation of stromal collagen fibers affected δδ2 and δδ3, there were no significant differences in collagen fiber density between the low-responders and high-responders. This limitation may be due to non-specific chemotherapy-induced fibrosis, and the presence of various types of collagen fibers, such as types I, II, III, V, VI, XI, XXIV and XXVII (34). Collagen fiber subtypes cannot be identified using Masson's trichrome staining. In the present study, to prioritize visualization, Masson's trichrome staining, not immunostaining, was used (23). Second, there was some concern that necrotic, fibrous and severe inflammatory cancer tissue would affect the results of TDC. In the present study, it was difficult to visualize the cancer microenvironment using CT images, which is a technical limitation. It may be hypothesized that a novel radiological technique, such as dual-energy CT, would solve this problem, and this may be a topic of future research. Third, there were no prognostic significant differences between the ART grading system, δδ2 and δδ3 in recurrence-free survival. This may be attributed to the impacts of drug types and dosing periods that were not considered in the present study because of the limited number of patients. Studies with larger sample sizes should be conducted in the future to minimize these limitations.

In conclusion, the histological differences in PDAC between the NAC and non-NAC groups were identified, and the use of TDCs of dynamic CECT for the prediction of the histological therapeutic effects of NAC was suggested. However, it remains difficult to draw firm conclusions because the present study lacked a larger cohort. Novel research and radiological techniques, and a large cohort may allow for the integration of radiological and histological analyses in future research.

Acknowledgements

The authors would like to thank the following research assistants: Ms. Misaki Ishiyama (Hirosaki University School of Medicine), Ms. Shizuka Fujio (Hirosaki University School of Medicine), Ms. Yuri Nakano (Hirosaki University School of Medicine) and Mr. Yuya Takami (Hirosaki University School of Medicine).

Funding

The present study was supported by JSPS KAKENHI (grant no. JP19K16763).

Availability of data and materials

The datasets used and/or analyzed during the current study are available from the corresponding author on reasonable request.

Authors' contributions

SG and TY designed the experiments. SG performed the experiments and data analysis, wrote the main manuscript and prepared the figures. HS evaluated the radiological images. SM and HK contributed to histological evaluation. HO, SK, KO, AN, KI and KH provided clinical information and interpreted clinical data. TY and HK confirm the authenticity of all the raw data. All authors read and approved the final manuscript, and agree to be accountable for all aspects of the research in ensuring that the accuracy or integrity of any part of the work are appropriately investigated and resolved.

Ethics approval and consent to participate

The research protocol was approved by the ethics committee of Hirosaki University (approval no. 2022-035). All study procedures involving human participants were performed in accordance with the ethical standards of the institutional and/or national research committee and with the 1964 Helsinki Declaration and its later amendments or comparable ethical standards. Written informed consent for the use of clinical records and pathological specimens was obtained from each patient before commencement of the study.

Patient consent for publication

Not applicable.

Competing interests

The authors declare that they have no competing interests.

References

1. Burris HA III, Moore MJ, Andersen J, Green MR, Rothenberg ML, Modiano MR, Cripps MC, Portenoy RK, Storniolo AM, Tarassoff P, *et al*: Improvements in survival and clinical benefit with gemcitabine as first-line therapy for patients with advanced pancreas cancer: A randomized trial. J Clin Oncol 15: 2403-2413, 1997.
2. Whatcott CJ, Diep CH, Jiang P, Watanabe A, LoBello J, Sima C, Hostetter G, Shepard HM, Von Hoff DD and Han H: Desmoplasia in primary tumors and metastatic lesions of pancreatic cancer. Clin Cancer Res 21: 3561-3568, 2015.
3. Neesse A, Bauer CA, Öhlund D, Lauth M, Buchholz M, Michl P, Tuveson DA and Gress TM: Stromal biology and therapy in pancreatic cancer: Ready for clinical translation? Gut 68: 159-171, 2019.
4. Oba A, Ho F, Bao QR, Al-Musawi MH, Schulick RD and Del Chiaro M: Neoadjuvant treatment in pancreatic cancer. Front Oncol 10: 245, 2020.
5. Motoi F and Unno M: Adjuvant and neoadjuvant treatment for pancreatic adenocarcinoma. Jpn J Clin Oncol 50: 483-489, 2020.

6. Versteijne E, van Dam JL, Suker M, Janssen QP, Groothuis K, Akkermans-Vogelaar JM, Besselink MG, Bonsing BA, Buijsen J, Busch OR, *et al*: Neoadjuvant chemoradiotherapy versus upfront surgery for resectable and borderline resectable pancreatic cancer: Long-term results of the Dutch randomized PREOPANC trial. J Clin Oncol 40: 1220-1230, 2022.
7. Von Hoff DD, Ervin T, Arena FP, Chiorean EG, Infante J, Moore M, Seay T, Tjulandin SA, Ma WW, Saleh MN, *et al*: Increased survival in pancreatic cancer with nab-paclitaxel plus gemcitabine. N Engl J Med 369: 1691-1703, 2013.
8. Goldstein D, El-Maraghi RH, Hammel P, Heinemann V, Kunzmann V, Sastre J, Scheithauer W, Siena S, Tabernero J, Teixeira L, *et al*: nab-Paclitaxel plus gemcitabine for metastatic pancreatic cancer: Long-term survival from a phase III trial. J Natl Cancer Inst 107: dju413, 2015.
9. Welsh JL, Bodeker K, Fallon E, Bhatia SK, Buatti JM and Cullen JJ: Comparison of response evaluation criteria in solid tumors with volumetric measurements for estimation of tumor burden in pancreatic adenocarcinoma and hepatocellular carcinoma. Am J Surg 204: 580-585, 2012.
10. Chatterjee D, Katz MH, Rashid A, Wang H, Iuga AC, Varadhachary GR, Wolff RA, Lee JE, Pisters PW, Crane CH, *et al*: Perineural and intraneural invasion in posttherapy pancreaticoduodenectomy specimens predicts poor prognosis in patients with pancreatic ductal adenocarcinoma. Am J Surg Pathol 36: 409-417, 2012.
11. Lee SM, Katz MH, Liu L, Sundar M, Wang H, Varadhachary GR, Wolff RA, Lee JE, Maitra A, Fleming JB, *et al*: Validation of a proposed tumor regression grading scheme for pancreatic ductal adenocarcinoma after neoadjuvant therapy as a prognostic indicator for survival. Am J Surg Pathol 40: 1653-1660, 2016.
12. Kalimuthu SN, Serra S, Dhani N, Hafezi-Bakhtiari S, Szentgyorgyi E, Vajpeyi R and Chetty R: Regression grading in neoadjuvant treated pancreatic cancer: An interobserver study. J Clin Pathol 70: 237-243, 2017.
13. Matsuda Y, Ohkubo S, Nakano-Narusawa Y, Fukumura Y, Hirabayashi K, Yamaguchi H, Sahara Y, Kawanishi A, Takahashi S, Arai T, *et al*: Objective assessment of tumor regression in post-neoadjuvant therapy resections for pancreatic ductal adenocarcinoma: Comparison of multiple tumor regression grading systems. Sci Rep 10: 18278, 2020.
14. Ferrone CR, Marchegiani G, Hong TS, Ryan DP, Deshpande V, McDonnell EI, Sabbatino F, Santos DD, Allen JN, Blaszkowsky LS, *et al*: Radiological and surgical implications of neoadjuvant treatment with FOLFIRINOX for locally advanced and borderline resectable pancreatic cancer. Ann Surg 261: 12-17, 2015.
15. Wagner M, Antunes C, Pietrasz D, Cassinotto C, Zappa M, Sa Cunha A, Lucidarme O and Bachet JB: CT evaluation after neoadjuvant FOLFIRINOX chemotherapy for borderline and locally advanced pancreatic adenocarcinoma. Eur Radiol 27: 3104-3116, 2017.
16. Goto S, Seino H, Yoshizawa T, Morohashi S, Ishido K, Hakamada K and Kijima H: Time density curve of dynamic contrast-enhanced computed tomography correlates with histological characteristics of pancreatic cancer. Oncol Lett 21: 276, 2021.
17. Brierley JD, Gospodarowicz MK and Wittekind C (eds): The TNM classification of malignant tumours, 8th edition. Wiley-Blackwell, Oxford, pp93-95, 2017.
18. WHO Classification of Tumours Editorial Board: WHO classification of tumours of the digestive system. IARC Press, Lyon, pp322-332, 2019.
19. Inoue C, Miki Y, Saito R, Hata S, Abe J, Sato I, Okada Y and Sasano H: PD-L1 induction by cancer-associated fibroblast-derived factors in lung adenocarcinoma cells. Cancers (Basel) 11: 1257, 2019.
20. Itou RA, Uyama N, Hirota S, Kawada N, Wu S, Miyashita S, Nakamura I, Suzumura K, Sueoka H, Okada T, *et al*: Immunohistochemical characterization of cancer-associated fibroblasts at the primary sites and in the metastatic lymph nodes of human intrahepatic cholangiocarcinoma. Hum Pathol 83: 77-89, 2019.
21. Zhang J, Li S, Zhao Y, Ma P, Cao Y, Liu C, Zhang X, Wang W, Chen L and Li Y: Cancer-associated fibroblasts promote the migration and invasion of gastric cancer cells via activating IL-17a/JAK2/STAT3 signaling. Ann Transl Med 8: 877, 2020.
22. Matsuda K, Ohga N, Hida Y, Muraki C, Tsuchiya K, Kurosu T, Akino T, Shih SC, Totsuka Y, Klagsbrun M, *et al*: Isolated tumor endothelial cells maintain specific character during long-term culture. Biochem Biophys Res Commun 394: 947-954, 2010.
23. Calvi EN, Nahas FX, Barbosa MV, Calil JA, Ihara SS, Silva Mde S, Franco MF and Ferreira LM: An experimental model for the study of collagen fibers in skeletal muscle. Acta Cir Bras 27: 681-686, 2012.
24. Kanda Y: Investigation of the freely available easy-to-use software 'EZR' for medical statistics. Bone Marrow Transplant 48: 452-458, 2013.
25. Miyashita T, Tajima H, Makino I, Okazaki M, Yamaguchi T, Ohbatake Y, Nakanuma S, Hayashi H, Takamura H, Ninomiya I, *et al*: Neoadjuvant chemotherapy with gemcitabine plus nab-paclitaxel reduces the number of cancer-associated fibroblasts through depletion of pancreatic stroma. Anticancer Res 38: 337-343, 2018.
26. Mancini ML and Sonis ST: Mechanisms of cellular fibrosis associated with cancer regimen-related toxicities. Front Pharmacol 5: 51, 2014.
27. Arimoto A, Uehara K, Tsuzuki T, Aiba T, Ebata T and Nagino M: Role of bevacizumab in neoadjuvant chemotherapy and its influence on microvessel density in rectal cancer. Int J Clin Oncol 20: 935-942, 2015.
28. Eefsen RL, Engelholm L, Willemoe GL, Van den Eynden GG, Laerum OD, Christensen IJ, Rolff HC, Høyer-Hansen G, Osterlind K, Vainer B and Illemann M: Microvessel density and endothelial cell proliferation levels in colorectal liver metastases from patients given neo-adjuvant cytotoxic chemotherapy and bevacizumab. Int J Cancer 138: 1777-1784, 2016.
29. Awai K and Date S: Basic knowledge to achieve optimal enhancement of CT. Nichidoku Iho 56: 13-32, 2011.
30. Harder FN, Jungmann F, Kaissis GA, Lohöfer FK, Ziegelmayer S, Havel D, Quante M, Reichert M, Schmid RM, Demir IE, *et al*: [18F]FDG PET/MRI enables early chemotherapy response prediction in pancreatic ductal adenocarcinoma. EJNMMI Res 11: 70, 2021.
31. Hamdy A, Ichikawa Y, Toyomasu Y, Nagata M, Nagasawa N, Nomoto Y, Sami H and Sakuma H: Perfusion CT to assess response to neoadjuvant chemotherapy and radiation therapy in pancreatic ductal adenocarcinoma: Initial experience. Radiology 292: 628-635, 2019.
32. Abdelrahman AM, Goenka AH, Alva-Ruiz R, Yonkus JA, Leiting JL, Graham RP, Merrell KW, Thiels CA, Hallemeier CL, Warner SG, *et al*: FDG-PET predicts neoadjuvant therapy response and survival in borderline resectable/locally advanced pancreatic adenocarcinoma. J Natl Compr Canc Netw 20: 1023-1032.e3, 2022.
33. Koay EJ, Truty MJ, Cristini V, Thomas RM, Chen R, Chatterjee D, Kang Y, Bhosale PR, Tamm EP, Crane CH, *et al*: Transport properties of pancreatic cancer describe gemcitabine delivery and response. J Clin Invest 124: 1525-1536, 2014.
34. Myllyharju J and Kivirikko KI: Collagens and collagen-related diseases. Ann Med 33: 7-21, 2001.